Copper Bipyridyl Redox Mediators for Dye-Sensitized Solar Cells with High Photovoltage

Yasemin Saygili,[†] Magnus Söderberg,[‡] Norman Pellet,[§] Fabrizio Giordano,[§] Yiming Cao,[§] Ana Belen Muñoz-García,[∥] Shaik M. Zakeeruddin,[†] Nick Vlachopoulos,[†] Michele Pavone,[∥] Gerrit Boschloo,[⊥] Ladislav Kavan,[§,#] Jacques-E. Moser,[‡] Michael Grätzel,[§] Anders Hagfeldt,[†] and Marina Freitag*,[†,⊥]

[†]Laboratory of Photomolecular Science, [‡]Photochemical Dynamics Group, and [§]Laboratory for Photonics and Interfaces, Institute of Chemical Sciences Engineering, École Polytechnique Fédérale de Lausanne, 1015 Lausanne, Switzerland

[∥]Department of Chemical Sciences, University of Naples Federico II, 80126 Naples, Italy

[⊥]Department of Chemistry, Ångström Laboratory, Uppsala University, 751 20 Uppsala, Sweden

[#]J. Heyrovsky Institute of Physical Chemistry, 1823 Prague, Czech Republic

S *Supporting Information*

ABSTRACT: Redox mediators play a major role determining the photocurrent and the photovoltage in dye-sensitized solar cells (DSCs). To maintain the photocurrent, the reduction of oxidized dye by the redox mediator should be significantly faster than the electron back transfer between TiO_2 and the oxidized dye. The driving force for dye regeneration with the redox mediator should be sufficiently low to provide high photovoltages. With the introduction of our new copper complexes as promising redox mediators in DSCs both criteria are satisfied to enhance power conversion efficiencies. In this study, two copper bipyridyl complexes, $Cu^{(II/I)}(dmby)_2TFSI_{2/1}$ (0.97 V vs SHE, dmby = 6,6′-dimethyl-2,2′-bipyridine) and $Cu^{(II/I)}(tmby)_2TFSI_{2/1}$ (0.87 V vs SHE, tmby = 4,4′,6,6′-tetramethyl-2,2′-bipyridine), are presented as new redox couples for DSCs. They are compared to previously reported $Cu^{(II/I)}(dmp)_2TFSI_{2/1}$ (0.93 V vs SHE, dmp = bis(2,9-dimethyl-1,10-phenanthroline). Due to the small reorganization energy between Cu(I) and Cu(II) species, these copper complexes can sufficiently regenerate the oxidized dye molecules with close to unity yield at driving force potentials as low as 0.1 V. The high photovoltages of over 1.0 V were achieved by the series of copper complex based redox mediators without compromising photocurrent densities. Despite the small driving forces for dye regeneration, fast and efficient dye regeneration (2−3 µs) was observed for both complexes. As another advantage, the electron back transfer (recombination) rates were slower with $Cu^{(II/I)}(tmby)_2TFSI_{2/1}$ as evidenced by longer lifetimes. The solar-to-electrical power conversion efficiencies for $[Cu(tmby)_2]^{2+/1+}$, $[Cu(dmby)_2]^{2+/1+}$, and $[Cu(dmp)_2]^{2+/1+}$ based electrolytes were 10.3%, 10.0%, and 10.3%, respectively, using the organic Y123 dye under 1000 W m^{-2} AM1.5G illumination. The high photovoltaic performance of Cu-based redox mediators underlines the significant potential of the new redox mediators and points to a new research and development direction for DSCs.
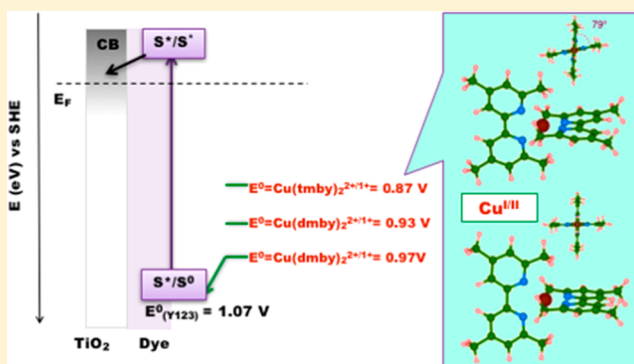
INTRODUCTION

The drastic increase in worldwide energy demand combined with climate change has shifted interest in the past half-century toward renewable energy sources. Solar energy systems, including photovoltaics, show a rapid increase in development and industrialization and constitute to a very significant part in the field of renewable energy research. Dye-sensitized solar cells (DSC) achieve direct sunlight-to-electricity conversion by partially mimicking photosynthesis, rendering it a unique photovoltaic technology.[1] This system offers a promising alternative to manufacture highly efficient solar cells in every color imaginable, including transparency made from environmentally friendly and very cost-efficient materials.[2]

In a DSC, dye molecules are anchored to a mesoscopic wide band gap semiconductor surface. Following light absorption, the photoexcited dye molecules inject electrons into the conduction band of the semiconductor (typically TiO_2). The oxidized dye molecules are regenerated by a hole transport material, either a solid hole conductor or a liquid redox system, while the electrons injected into TiO_2 provide electric work in the external circuit. The cycle is completed by the reduction of the oxidized redox species at a catalyst-loaded counter electrode surface. Since the discovery of DSCs, the iodide/tri-iodide
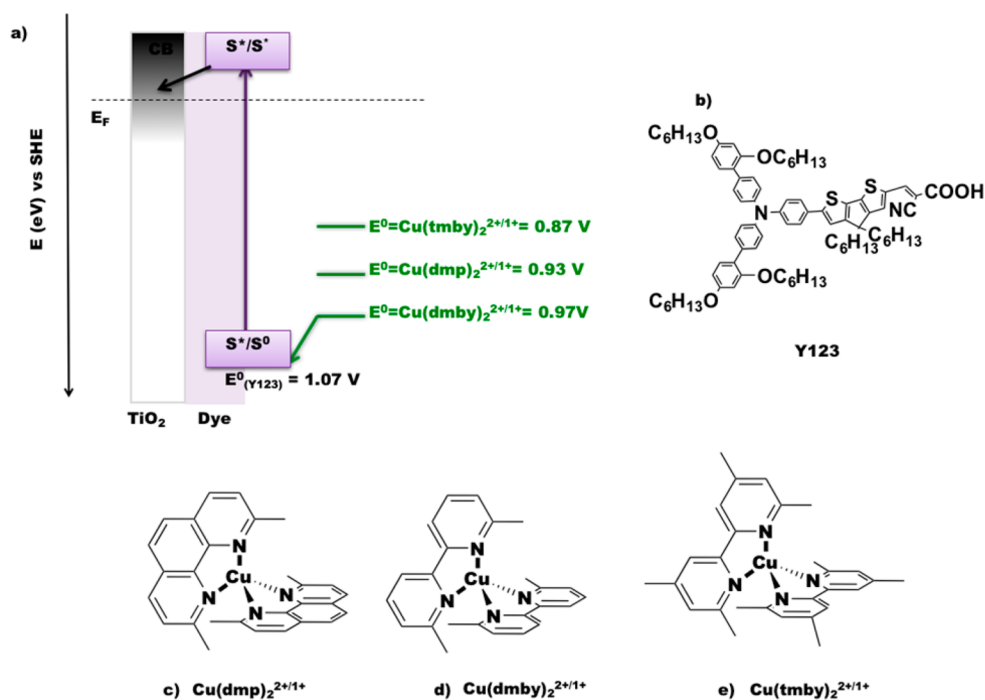
Figure 1. (a) Schematic representation of energy levels in dye-sensitized solar cells. Molecular structures of the (b) Y123 dye, (c) $Cu(dmp)_2]^{2+/1+}$, (d) $[Cu(dmby)_2]^{2+/1+}$, and (e) $[Cu(tmby)_2]^{2+/1+}$ complexes.

redox couple has been conventionally used as the redox mediator, which has shown the highest efficiency values together with excellent stability data with different types of sensitizers in comparison to other redox mediators.[2] The main advantage of this redox couple is the suppressed recombination of injected electrons with tri-iodide providing high photocurrents. However, being a two-electron redox couple, I^-/I_3^- electrolytes cause large internal potential losses for oxidized dye regeneration. In addition, there may be problems of corrosiveness and competitive visible light absorption.[3,4] These disadvantages were overcome with one-electron-transfer cobalt complexes with more positive redox potentials, which resulted in an improved photovoltage and with overall higher efficiencies compared to those of the I^-/I_3^- system.[5−7] In these complexes, different ligand substitutions to the cobalt metal center enable the tuning of the redox potentials and electron transfer kinetics. So far, the highest efficiency value achieved is claimed to be above 14% for liquid-state DSCs with cobalt redox-mediator based electrolyte and dye-cosensitized working electrode.[8] However, the large internal reorganization energy requirement between d^7 (high spin) and d^6 (low spin) states for cobalt complexes turns out to be a disadvantage by limiting the driving force available for dye regeneration.[9] The necessary driving force for dye regeneration was reported to be 230 mV in order to achieve a 93% regeneration yield with a triphenylamine-based organic dye[10] which still gives a substantial potential loss.[11,12] With a coordination number of six (octaheadral), the ligands linked to a cobalt metal center form bulky structures, leading to mass transport limitations in the mesoporous layer.[13−15] Stability issues and toxicity concerns regarding cobalt complexes limit their potential for industrialization and mass production.[16,17]

As alternative redox mediators, copper complexes (Cu(I)/Cu(II)) have been studied both as redox mediators[18−21] and hole-transport materials (HTMs)[22] in DSCs. First, Hattori et al. obtained a maximum photon to current efficiency (PCE) of

1.4% with bis(2,9-dimethyl-1,10-phenantroline)copper(I)/(II) $[Cu(dmp)_2]^{2+/+1}$, which has a distorted tetragonal shape providing a relatively low reorganization energy.[19] The results were further improved by Bai et al., who reached 7% PCE[18] with the organic C218 dye, and recently, Freitag et al. attained 8.3% PCE by having remarkably high open-circuit voltages (V_{oc}) above 1.0 V with the organic D−π−A LEG4 dye.[23] Furthermore, it was reported that the $[Cu(dmp)_2]^{2+/1+}$ complex with a redox potential of 0.93 V vs SHE is able to sufficiently regenerate the oxidized dye molecules with a small driving force (0.2 eV), minimizing internal energy losses.

Herein, we report two new copper bipyridine complexes, 6,6′-dimethyl-2,2′-bipyridine $(Cu^{(II/I)} (dmby)_2TFSI_{2/1})$ and 4,4′,6,6′-tetramethyl-2,2′-bipyridine $(Cu^{(II/I)} (tmby)_2TFSI_{2/1})$, which we examined in comparison to the reference $[Cu(dmp)_2]^{2+/1+}$ complex in DSCs sensitized with the 3-{6-{4-[bis(2′,4′-dihexyloxybiphenyl-4-yl)amino-]phenyl}-4,4-dihexylcyclopenta-[2,1-b:3,4-b′]dithiphene-2-yl}-2-cyanoacrylic (Y123) dye.[10,24] We tuned the formal redox potentials of copper complexes relative to $[Cu(dmp)_2]^{2+/1+}$ and investigated this change with respect to regeneration kinetics and device performance. By maintaining the coordination geometry around the copper metal center during the change of the Cu oxidation state from I to II, internal reorganization energies can be minimized, allowing the regeneration to proceed rapidly at low driving force. For Cu(I) bis-phenanthroline complexes, the non-hydrogen groups at 2,9-positions of phenanthroline ligand had already been reported to provide small changes in ligand-copper distances upon oxidation.[25−27]

Since $Cu(dmp)_2$ is already proven a successful redox mediator for DSCs, the $Cu(dmby)_2$ complex is similarly designed by keeping the methyl groups at 2,9-positions and replacing the phenanthroline with bipyridine to tune the redox potential and other properties. The structure of the $Cu(tmby)_2$ complex has two additional methyl groups at each ligand; the electron-donating effect of a methyl group (4,6-positions) shifts

the redox potential by 100 mV toward the negative. A schematic representation of the energy levels in DSC devices and molecular structures of the Y123 dye and the copper complexes are given in Figure 1. DSCs employing the new copper complexes as redox mediators reached photovoltages over 1.0 V in full sunlight allowing them to reach photoelectric conversion efficiency values higher than 10% for the complexes under study.

■ EXPERIMENTAL SECTION

All chemicals and solvents were purchased from Sigma-Aldrich, HetCat, and TCI Chemicals, if not otherwise stated, and were used without further purification.

Synthesis of Copper Complexes. The synthesis of copper complexes was performed as previously reported.[28] For (Cu-(dmp)$_2$TFSI) (Figure S1), 1 equiv of CuI was mixed with 4 equiv of neocuproine hydrate in ethanol, under nitrogen atmosphere, at room temperature for 2 h. The stirred solution was filtered and washed with water and diethyl ether. The resulting complex was collected as an intense red crystalline powder.

The Cu(dmp)$_2$TFSI$_2$ complex was produced by the oxidation of Cu(I) species with addition of NOBF$_4$. Briefly, Cu(dmp)$_2$TFSI was dissolved in acetonitrile and 1 equiv of NOBF$_4$, followed by 5 equiv of LiTFSI being added after 30 min.

The solution was further stirred for 2 h at room temperature and nitrogen atmosphere. The solvent was removed by rotatory evaporation and the crude redissolved in minimum amount of dichloromethane (DCM). Cu(dmp)$_2$TFSI$_2$ was collected by filtration after precipitation from diethyl ether and washed with diethyl ether. The product was a bright violet powder.

For complexation of Cu(dmby)$_2$TFSI and Cu(tmby)$_2$TFSI, 1 equiv of CuI was mixed with 3 equiv of dmby or tmby, respectively, in 20 mL of ethanol, under nitrogen atmosphere, at room temperature for 2 h (Figure S2). The resulting Cu(I) complexes were obtained as intense red crystalline powders. The Cu(I) products were filtered and redissolved by addition of 5 mL of deionized water followed by an addition of 5 equiv of LiTFSI. The solutions were further stirred for 2 h at room temperature under nitrogen atmosphere resulting in red precipitations. The complexes were collected by filtration and washed with water as bright red powders.

For Cu(dmby)$_2$TFSI$_2$ and Cu(tmby)$_2$TFSI$_2$ 1 equiv of CuCl$_2$ was mixed with 3 equiv of dmby or tmby, respectively, in 20 mL of ethanol, under nitrogen atmosphere, at room temperature for 2 h. The resulting complexes were obtained as green powders. The product Cu(II) species were filtered and redissolved by addition of 5 mL of deionized water followed by an addition of 5 equiv of LiTFSI. The solution was further stirred for 2 h at room temperature and under nitrogen atmosphere. The complexes were collected by filtration as green powders and washed with water.

Electrochemical Characterization. Three-electrode cyclic voltammetry measurements were performed using a Autolab Pgstat-30 potentiostat with a Ag/AgCl/saturated LiCl (ethanol) as reference electrode and glassy carbon or platinum working electrodes under argon. Copper complexes were dissolved in acetonitrile, with LiTFSI (0.1M) as supporting electrolyte. Redox potentials were primarily referenced versus ferrocene, which was added *in situ* as voltammetric standard. The formal potential of Fc/Fc$^+$ couple was between 0.468 and 0.471 V vs our Ag/AgCl reference electrode.

Diffusion coefficient measurements were performed via rotating disk electrode voltammetry. A Bio Logic SP300 potentiostat with a quasi-reference platinum electrode and glassy carbon rotating disk electrode (2.9 mm, Radiometer Analytical-CVJ) was used in a solution of 0.1 M LiTFSI and 0.5 M 4-*tert*-butylpyridine (TBP) in acetonitrile under argon atmosphere. The rotor speed was controlled by a speed control unit (Radiometer Analytical-CTV101). The cell temperature was kept constant at 25 °C by a circulating water bath (HAAKE GH).

UV/vis absorption data were gathered by a Hewlett-Packard 8453 diode array spectrometer, and the extinction coefficients were calculated using the Lambert–Beer Law.

Device Fabrication. *Preparation of the Working Electrodes.* The photoanodes with a mesoporous TiO$_2$ layer, counter electrodes, and electrolytes were prepared separately and then assembled in a solar cell device. For photoanodes, a glass pretreatment procedure was followed to remove the contaminations that can affect the preparation of the compact underlayer and thus the cell performance. FTO glasses (NSG-10, Nippon Sheet Glass) were first cleaned with a detergent solution (Deconex) in ultrasonic bath (45 min) and rinsed with water and ethanol. This initial step was followed by a 15 min UV/O$_3$ treatment (Model no.256–220, Jelight Company, Inc.). Then the substrates were immersed into a 53 mM TiCl$_4$ solution and kept at 70 °C in an oven for 30 min to allow the formation of thin and compact TiO$_2$ underlayer. After 30 min the substrates were rinsed with water and ethanol. The TiCl$_4$ treatment was followed by a 2 h annealing process at 250 °C. Two layers of mesoporous TiO$_2$ layers were prepared on top of the underlayer; the first layer was screen printed using a paste consisting of 30 nm in diameter sized TiO$_2$ particles (Dyesol) and the second one with 400 nm sized particles (scattering layer). The substrates were sintered on a hot plate with a ramped temperature profile, keeping the temperature at 125, 250, 325, 450, and 500 °C for 5, 5, 5, 15, and 15 min, respectively, with 5 min ramp duration between each temperature. The resulting TiO$_2$ film thickness was 10 μm (5 μm + 5 μm). To increase the surface area of the TiO$_2$ particles, a TiCl$_4$ post-treatment was performed, which was followed by another sintering process at 500 °C for 30 min. Before dipping the TiO$_2$ electrodes into dye solutions, they were annealed with a hot gun for 30 min at 500 °C. After cooling down to 80 °C, they were put into the dye solution.

Dye Solutions. Y123 dye (Dyenamo AB, 0.1 mM) solutions were prepared in *tert*-butanol/acetonitrile (1:1 v/v) mixture; 0.4 mM chenodeoxycholic acid was used in the dye solutions as an additive to prevent aggregation. Working electrodes were dipped for 16 h in these solutions.

Preparation of the Counter Electrodes. FTO glass (TEC 6, Pilkington) as substrate for the counter electrodes was cleaned with Deconex (2% wt in water), acetone, and ethanol with 30 min duration for each and coated with PEDOT via electrodeposition.[29]

The working electrodes and counter electrodes were assembled in a drybox with 25 μm of Surlyn (Dupont), which provides the spacing between the two electrodes as well as sealing for the electrolyte. The electrolyte was introduced into the device through a predrilled hole in the counter electrode under vacuum. The electrolytes consisted of 0.2 M Cu(I) and 0.04 M Cu(II) complexes with 0.1 M LiTFSI and 0.6 M TBP in acetonitrile.

Solar Cell Characterization. The device current–voltage (I−V) characteristics were obtained by using a 450W xenon light source (Oriel, U.S.A). A Keithley model 2400 digital source meter (Keithley, U.S.A) was used to apply an external potential bias to the devices and measure the resulting current.

Incident Photon to Current Conversion Efficiency (IPCE). IPCE data were acquired using a modulated light intensity with a frequency of 1 Hz. The light, from a 300 W xenon light source (ILC Technology, USA), was focused through a monochromator (JobinYvon Ltd., UK) and directed to the device under test. A white light bias was used to have similar light intensity conditions as during normal operation.

Electron Lifetime Measurements. Electron lifetime measurements were performed using a white LED (Luxeon Star 1W) as light source. Voltage traces were recorded with a 16-bit resolution digital acquisition board (National Instruments) and lifetimes were determined by monitoring photovoltage transients at different light intensities upon applying a small square wave modulation to the base light intensity. The photovoltage responses were fitted using first-order kinetics to obtain time constants.

Photoinduced Absorption Spectroscopy (PIA). The photoinduced absorption spectra of the various cells were recorded over a wavelength range of 450–1000 nm following an (on/off) photomodulation using a 36 Hz square wave emanating from a blue laser (406 nm) filter through a notch (Balzers 405). White probe light from a halogen lamp (20 W) was used as an illumination source. The light

Table 1. Electrochemical and Absorption Data for Cu(I) and Cu(II) Species[a]

	ε (M^{-1} cm^{-1})	λ_{max} (nm)	D ($\times 10^{-6}$ cm^2 s^{-1})	$E^{0\prime\prime}$ (V vs SHE)
Cu(I) (dmp)$_2$TFSI	7300	457	12.6	0.93
Cu(II) (dmp)$_2$(TFSI)$_2$	850	360	14.4	
Cu(I) (dmby)$_2$TFSI	6900	455	11.7	0.97[b]
Cu(II) (dmby)$_2$TFSI/Cl	1300	360	33.3	
Cu(I) (tmby)$_2$TFSI	5300	451	11.2	0.87[b]
Cu(II) (tmby)$_2$TFSI/Cl	1400	360	22.0	

[a]ε: extinction coefficient, λ_{max} = absorption peak wavelength, D: diffusion coefficient, $E^{0\prime\prime}$: formal redox potential) [b]These formal potentials are determined from the voltammogram of Cu(I) species only.
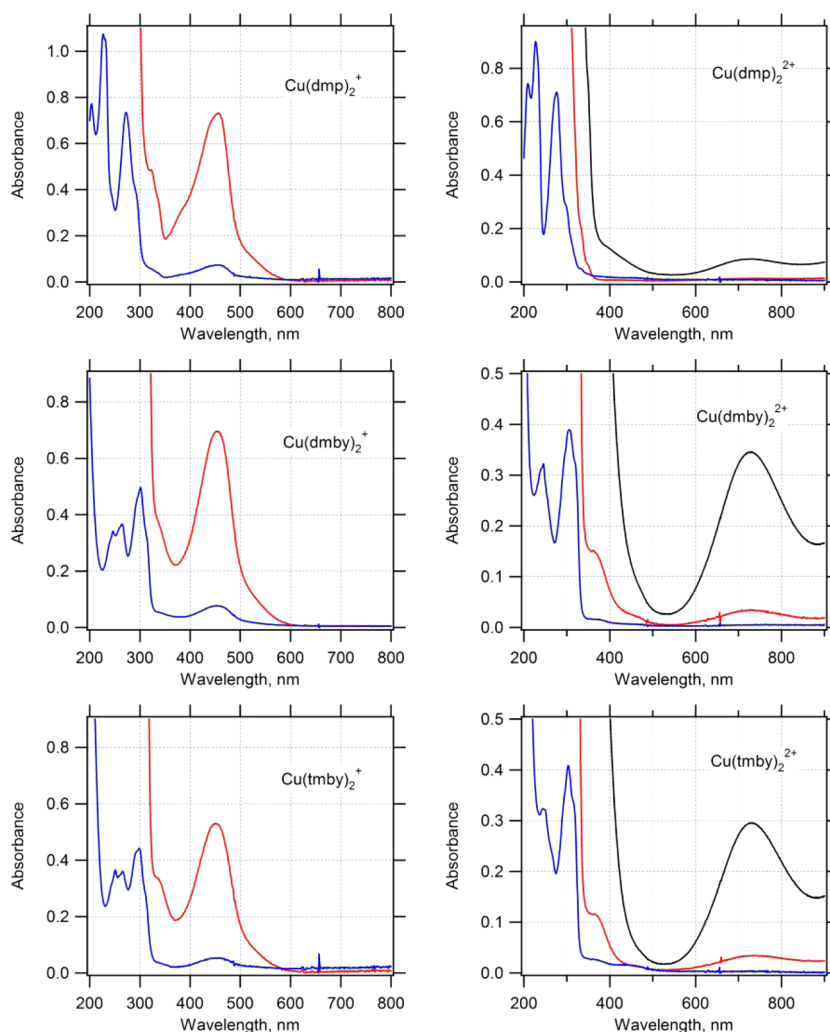

Figure 2. UV–vis spectra of CuL$_2$TFS I$_{1/2}$ (L = ligand) in acetonitrile solution; concentration: 50 μM (blue curves), 0.5 mM (red curves), and 5 mM (black curves). Optical cell thickness 2 mm.

was focused into a monochromator (Horiba, Gemini) and detected using a Si photodiode with a gain of 10, connected to a lock-in amplifier (Stanford Research Systems model SR830).

Transient Absorption Spectra (TAS). The photoinduced kinetics were measured with an Ekspla NT-342 Q-switched Nd:YAG laser using 532 nm as excitation wavelength. The pulse width was 4–5 ns (FWHM), and the repetition rate was 20 Hz. The probe light source was a halogen lamp, and the probe wavelength at 715 nm was chosen using a monochromator. The film was positioned at approximately 45° angle with respect to the incoming laser pulse for front illumination. The signal was detected using the photomultiplier tube R9110 from Hamamatsu and recorded using the oscilloscope DPO 7254 from Tektronix. The radiant output of the laser was attenuated using gray optical density filters to 46 μJ/cm^2 for the measurements of the

samples containing redox mediators and 1.27 μJ/cm^2 for the electrolytically inert samples. A low light intensity value was deliberately chosen in order to ensure that the data could be fitted to single exponential functions from which the lifetimes could be obtained. An acquisition was averaged over 3000 laser shots.

■ RESULTS AND DISCUSSION

Electrochemical and Spectroscopic Data. The formal redox potentials, extinction coefficients and diffusion coefficients of the investigated complexes, are tabulated in Table 1. The formal redox potentials of the $[Cu(dmby)_2]^{2+/1+}$ and $[Cu(tmby)_2]^{2+/1+}$ complexes are determined by cyclic voltam-
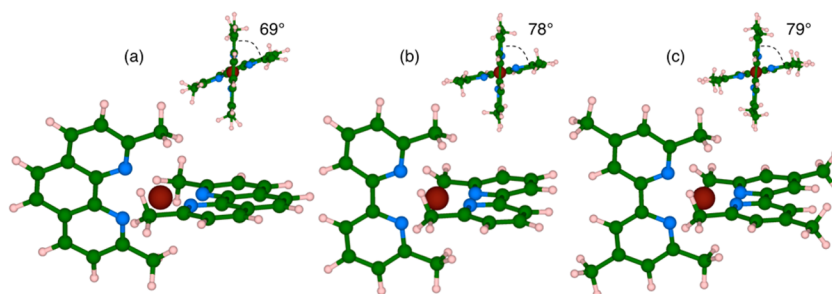
Figure 3. Cu(II) L_2 minimum-energy structures. L = dmp (a), dmby (b), and tmby (c).

metry using a three-electrode setup with a glassy carbon working electrode.

From the obtained reversible voltammograms (with equal anodic and cathodic peak currents after repeated cycles) of Cu(1) species, the formal (conditional) redox potentials for $[Cu(dmby)_2]^{2+/1+}$ and $[Cu(tmby)_2]^{2+/1+}$ are determined. If we omit the difference in activity coefficients, then the potentials can be approximated to the standard electrochemical potential, with 0.97 and 0.87 V vs the standard hydrogen electrode (SHE) for $[Cu(dmby)_2]^{2+/1+}$ and $[Cu(tmby)_2]^{2+/1+}$, respectively. The redox potentials were referenced to SHE by addition of 0.624 V with respect to the formal potential of the reference ferrocene/ferrocenium redox couple (Figure S3).

The different substitutions of the bipyridine ligands have an explicit influence on the redox potential of the complexes. The dimethyl substitution of the bipyridine ligands provides a higher redox potential for $[Cu(dmby)_2]^{2+/1}$, whereas the additional two methyl groups giving the electron donation function lower the redox potential for $[Cu(tmby)_2]^{2+/1+}$. The redox potential of $[Cu(dmp)_2]^{2+/1+}$ has been reported to be 0.94 V vs SHE.[28]

In the case of $[Cu(tmby)_2]^{2+}$ and $[Cu(dmby)_2]^{2+}$ species, we observe more complex voltammograms with negative shifts against the redox wave of $[Cu(tmby)_2]^{1+}$ and $[Cu(dmby)_2]^{1+}$. Solely in the case of phenanthroline complex, the formal redox potentials of Cu(II) and Cu(I) species were matching. To address this issue furthermore, an additional study was carried out, in which the Cu(dmby)$^{2+}$ and Cu(tmby)$^{2+}$ were back-reduced chemically, either by ferrocene or by ascorbic acid. In all cases, simple voltammograms of Cu(I) species were obtained, which points out the purity of the Cu(II) complexes (Figure S4). The reduction of Cu(tmby)$^{2+}$ by ferrocene caused precipitation in the electrolyte solution so that the voltammogram cannot be considered quantitative, but an upshift of the redox waves of the reduction product is obvious (Figure S4). A more elegant way of reducing Cu(tmby)$^{2+}$ to Cu(tmby)$^{1+}$ is the use of ascorbic acid (Figure S4). The electrochemical data shows that the reaction of CuCl$_2$ with the corresponding ligand provides more complex products than originally assumed. It can be assumed that the TFSI anion is coordinating to Cu(II) center, leading to the two species deferring in redox potentials. In contrast, the chemical oxidation of Cu(dmp)$^+$ by NOBF$_4$ provided a single species as shown in Figure S3a.

In a more recent work by Hupp and co-workers, TiO$_2$ conduction band edge shifts were attributed to the result of the coordination changes of the copper species due to excess TBP.[30] In addition to standard electrochemical potential determinations, cyclic voltammetry experiments were also performed in excess TBP conditions (2.5 times higher molar excess of TBP referenced to Cu(I), similar to the electrolyte

solution). In the case of excess TBP, significant negative shifts (about 20 mV) in the redox potentials were observed for the three investigated complexes, which also enhance the dye regeneration efficiencies by the increased driving forces (Figure S3).

The absorption spectra of Cu(I) (tmby)$_2$, Cu(I) (dmby)$_2$, and Cu(I) (dmp)$_2$ show absorption maxima at λ_{max} = 450−460 nm in acetonitrile, attributed to the metal-to-ligand charge transfer (MLCT) transitions (Figure 2 and S5). For Cu(II) species, the absorption peaks are observed in the UV region assigned to $\pi \rightarrow \pi^*$ transitions (Figure 2).

To compare the diffusion coefficients of the copper complexes, rotating disk electrode measurements were carried out. The results were analyzed with the use of the Koutecky−Levich equation. It is observed that copper complexes have higher diffusion coefficients in comparison to that of cobalt trisbipyridine complex. Each copper atom (with coordination number 4) is chelated with 2 ligands, whereas cobalt complexes (coordination number of 6) require 3 ligands. The copper complexes have smaller molecular size and therefore higher diffusion coefficients and thus can easily diffuse in the mesoporous structure. The diffusion coefficients for Co(III) (bpy)$_3$(TFSI)$_3$ and Co(II) (bpy)$_3$(TFSI)$_2$ were determined to be 7.2×10^{-6} and 6.1×10^{-6} cm^2 s^{-1}, respectively, under the same experimental conditions.

Density Functional Theory Calculations (DFT). In order to estimate the reaction free energies and internal reorganization energies for the three copper complexes, we performed DFT calculations with the Gaussian 09 suite of programs[31] at the PBE0 level of theory[32] with SDD ECP as basis set for Cu and TZVP basis set for other atoms. Structural optimizations, molecular frequencies, and thermochemistry data were obtained in solution with the polarizable continuum model (PCM) for acetonitrile.[33,34] Vertical excitation energies have been computed with time-dependent DFT (TD-DFT) at the same level of theory.[35]

For the three copper(I) complexes, HOMO and LUMO are both doubly degenerate. For $[Cu(dmp)_2]^{1+}$, the computed first electronic transition (ΔE_{exc}) at 466 nm (Table S1) corresponds to HOMO−LUMO transition and has a clear metal-to-ligand charge transfer character, Figure S6. The molecular orbitals for $[Cu(tmby)_2]^{1+}$ and $[Cu(dmby)_2]^{1+}$ present similar qualitative features.

According to the computations, copper(I) ligands stay in a perpendicular configuration (Figure S7), providing a tetrahedral coordination sphere for copper. Upon oxidation, the perpendicular alignment decays to a distorted tetragonal structure (Figure 3 and Table S2): The most favored square-planar Cu(II) coordination is prevented by the steric hindrance effects of the methyl groups in 2,9-positions of the ligands. The

free energy difference (ΔG_{ox}) for oxidation of copper species and the internal reorganization energies (λ_{in}) have been calculated for such configurations, and the results are listed in Table 2. These free energy values are qualitatively consistent

Table 2. Free Energy Differences for the Cu(I) → Cu(II) Process (ΔG_{ox}) and Corresponding Inner-Sphere Reorganization Energy (λ_{in})

	ΔG_{ox} (eV)	λ_{in} (eV)
$[Cu(dmp)_2]^{1+/2+}$	4.68	0.281
$[Cu(dmby)_2]^{1+/2+}$	4.64	0.301
$[Cu(tmby)_2]^{1+/2+}$	4.47	0.294
$[Co(bpy)_2]^{2+/3+}$ (low-spin)[36]	5.00	0.613

with the observed trend in experimental oxidation potentials. For the three copper complexes, the predicted inner-sphere reorganization energies are very low, about 0.3 eV, in comparison with those of cobalt species: For $Co(bpy)_3$ and related complexes, the λ_{in} values, computed with the same approach, lie in the range of 0.52–0.63 eV (considering Co(II) low spin) and 1.39–1.78 eV (for Co(II) high spin).[36] We have only addressed the internal (inner-sphere) reorganization energy because recent works from other groups[36,37] have proven that this parameter (λ_{in}) is the key feature limiting the overall dye regeneration process by Co-based redox mediators.

It is found that these low reorganization energy values for the copper complexes originate from very small changes in ligand-copper distances upon oxidation, which are only ~2% for Cu-ligand (against ~10% for Co-ligand complexes).[36] Moreover, the Cu(I) ion in its spherically symmetric $3d^{10}$ electronic configuration is less sensitive than Co(II) to structural distortions in the ligand coordination sphere. For copper complexes with the smaller reorganization energies, the driving force for dye regeneration can be kept small to obtain improved photovoltages.

Photovoltaic Performance of Dye-Sensitized Solar Cells with Copper Complexes. The photocurrent–voltage data of solar cells containing the three different copper redox mediators and Y123-sensitized TiO_2 films dye are given in Figure 4.
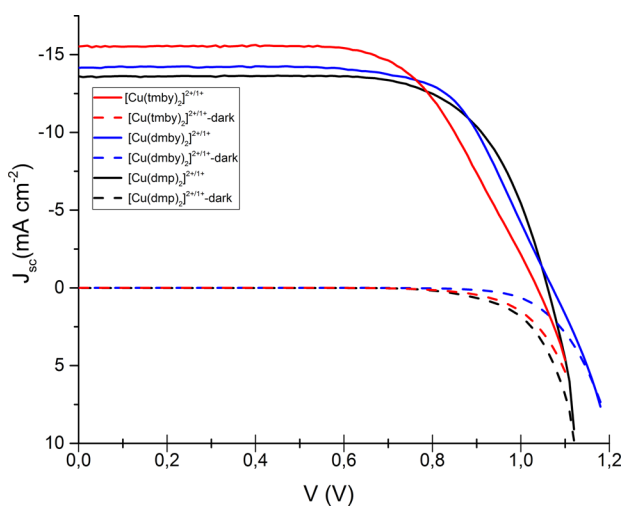
The photocurrent densities, open-circuit voltages, fill factors, and power conversion efficiencies of the DSC devices employing the $[Cu(tmby)_2]^{2+/1+}$, $[Cu(dmby)_2]^{2+/1+}$, and $[Cu(dmp)_2]^{2+/1+}$ complexes are summarized in Table 3 (see also

Table 3. I–V Characteristics for the $[Cu(dmp)_2]^{2+/1+}$, $[Cu(dmby)_2]^{2+/1+}$, and $[Cu(tmby)_2]^{2+/1+}$ Complexes

redox couple	V_{oc} (V)	J_{sc} (mA cm^{-2})	FF	PCE (%)
$[Cu(tmby)_2]^{2+/1+}$	1.04	15.53	0.640	10.3
$[Cu(dmby)_2]^{2+/1+}$	1.07	14.15	0.687	10.0
$[Cu(dmp)_2]^{2+/1+}$	1.06	13.61	0.692	10.3

Figures S8–10) The power conversion efficiency is calculated using

$$\eta = J_{sc} \times V_{oc} \times \frac{FF}{I_0} \quad (1)$$

where J_{sc} is the current density, V_{oc} is the open circuit voltage, FF is fill factor and I_0 is the incident light intensity. For all complexes, PCEs above 10% at AM 1.5 G illumination were reached. These are to our knowledge the highest PCEs reported for DSCs based on Cu complexes as redox mediators. The three redox couples show remarkably high open-circuit voltage values of more than 1.0 V at full sunlight illumination. Evidently, a regular trend between the formal redox potentials (Table 1) and the V_{oc} values was observed. Though the trend between V_{oc} and $E^{0\prime}$ is proportional, there are other effects to be taken into account in the discussion of the open circuit voltages of the DSCs. This will be further discussed below in relation to recombination and conduction band edge shifts with electron lifetimes and charge extraction measurements, respectively. The short-circuit current density is observed to be highest for the $[Cu(tmby)_2]^{2+/1+}$ electrolyte as a result of the highest driving force available for dye regeneration. Having the highest extinction coefficients for Cu(I), $[Cu(dmp)_2]^{1+/2+}$ complex shows the lowest short-circuit current density due to the competitive light absorbance.

The IPCE spectra for the DSC devices employing the three different redox couples are given in Figure 5. For $[Cu(tmby)_2]^{2+/1+}$ based electrolyte, the maximum IPCE is found to be 92% at 520 nm. For $[Cu(dmp)_2]^{2+/1+}$ and $[Cu-$

Figure 4. Photocurrent density vs voltage (J–V) curves measured under standard AM 1.5G illumination and in the dark for solar cells sensitized with Y123 dye and employing copper complexes.

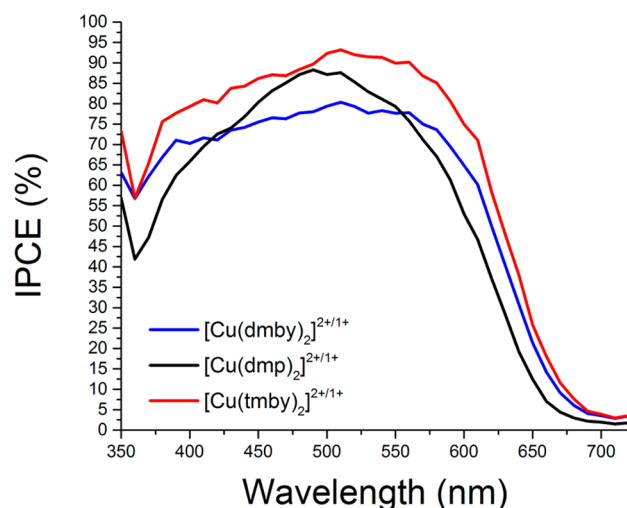**Figure 5.** IPCE spectra of DSC devices sensitized with Y123 dye.

(dmby)$_2$]$^{2+/1+}$, the maxima are 85 and 75%, respectively, around 500 nm. The drop of IPCE at 360 and 450 nm is ascribed to the absorption of Cu(I) and Cu(II) species in these regions. For further analysis, IPCE can be expressed as

$$IPCE = LHE\Phi_{inj}\eta_{coll} \qquad (2)$$

where LHE is light-harvesting efficiency, Φ_{inj} is the quantum yield of electron injection, and η_{coll} is the photogenerated charge collection efficiency. By assuming similar LHE and Φ_{inj} values (same dye and same working electrode parameters), the η_{coll} values can be compared for the copper complexes under study. The [Cu(tmby)$_2$]$^{2+/1+}$ electrolyte showed the best charge collection efficiencies due to the increased driving force for dye regeneration and presumably reduced recombination as indicated from electron lifetime measurements (electron lifetimes are measured under open circuit conditions). The broader IPCE spectrum for the [Cu(tmby)$_2$]$^{2+/1+}$ complex is attributed both to the electron collection yield due to longer electron lifetimes in the TiO$_2$ and lower extinction coefficient of this complex. The slightly blue-shifted IPCE of [Cu-(dmp)$_2$]$^{2+/1+}$ shows higher competitive light absorption for this complex.

Electron Lifetime Measurements. To understand the recombination reaction between the oxidized form of the redox species and injected electrons in TiO$_2$, electron lifetime and charge extraction measurements were carried out. Semilogarithmic plots of the measured electron lifetimes with respect to the quasi-Fermi level of the electrons in the TiO$_2$ electrode of the complete devices are given in Figure 6. At the
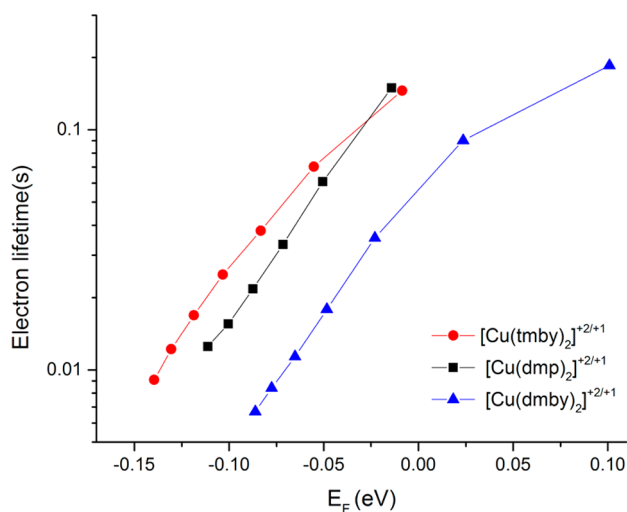

Figure 6. Electron lifetimes for the three copper complexes.

same Fermi level (-0.05 V vs SHE) the electron lifetimes were measured as 0.036, 0.021, and 0.006 s for the [Cu(tmby)$_2$]$^{2+/1+}$, [Cu(dmp)$_2$]$^{2+/1+}$, and [Cu(dmby)$_2$]$^{2+/1+}$, respectively. The electron lifetime values indicate that the recombination reaction is driving-force-dependent, corresponding to the Marcus normal region. The effect of steric properties of the ligands on the copper complexes is calculated to be similar to that for the recombination reaction due to similar reorganization energy values (Table 2) and therefore neglected. Electron lifetimes followed a coherent trend with respect to the driving force for recombination reaction. Since the driving force for recombination is the lowest in the case of [Cu(tmby)$_2$]$^{2+/1+}$ complex, the electron lifetime showed higher values in comparison to

those of other complexes. By having the most positive formal redox potential, the [Cu(dmby)$_2$]$^{2+/1+}$ complex resulted in lower electron lifetimes. The changes in the slopes of the electron lifetime data (see Figure 6) of the copper complexes is attributed to the recombination of electrons with FTO substrates at low currents. Preventing recombination at low currents can be achieved by better blocking layer processing and sensitizers with blocking properties.[38]

The fact that the V_{OC} values from the different Cu-complexes are similar, above 1.0 V, although the redox potentials differ by about 0.1 V, can be explained together by the differences in electron lifetimes and conduction band shifts. The V_{OC} value will be a compromise between driving force and recombination. For a larger driving force there will be a bigger internal potential drop between the redox potential of the electrolyte and the oxidation potential of the dye, leading to relatively lower V_{OC}. At the same time, dye regeneration will be faster and more efficient (see below). Faster dye regeneration will intercept the recombination reaction between electrons in the TiO$_2$ and oxidized dye and lead to a longer electron lifetime. This is an indication of higher electron concentration in the TiO$_2$, which means a higher quasi-Fermi level of the electrons and a relatively higher V_{OC}. Even if the [Cu(tmby)$_2$]$^{2+/1+}$ complex has a lower redox potential, 0.1 V lower compared to [Cu(dmby)$_2$]$^{2+/1+}$, the V_{OC} values are similar due to longer electron lifetimes for [Cu(tmby)$_2$]$^{2+/1+}$. The contribution of conduction band positions on V_{OC} can be observed via the charge extraction data. For the studied complexes, the charge extraction values normalized to Fermi level of the TiO$_2$ are given in Figure S11. At a certain value of extracted charge, the conduction band positions appeared to be most negative for [Cu(dmp)$_2$]$^{2+/1+}$ which is followed by [Cu(tmby)$_2$]$^{2+/1+}$ and [Cu(dmby)$_2$]$^{2+/1+}$. By having the most negative conduction band position and longer electron lifetimes, [Cu(dmp)$_2$]$^{2+/1+}$ could reach to V_{OC} values similar to the values of [Cu-(dmby)$_2$]$^{2+/1+}$ although the redox potential is lower. The differences in conduction band edges are attributed to the coordination changes due to TFSI and TBP especially for [Cu(tmby)$_2$]$^{2+}$ and [Cu(dmby)$_2$]$^{2+}$, in which the effect of coordination differences are clearly observable via cyclic voltammograms (Figure 3). The mechanism related to the coordination sphere changes will be studied later.

The light intensity dependence of the short circuit current density and photovoltage are given in Figure 7. The J_{SC} values showed a linear dependence for [Cu(tmby)$_2$]$^{2+/1+}$ complex. For the [Cu(dmp)$_2$]$^{2+/1+}$ and [Cu(dmby)$_2$]$^{2+/1+}$ complexes, the photocurrent deviates from linearity with increasing light intensities. This effect can be explained with mass transport limitations of the copper complexes. Under higher light intensities, diffusion problems gives rise to a higher internal series resistance. This will result in a nonlinear behavior of the photocurrent with light intensity as well as limitations of the fill factor in the DSC device. The high photovoltage stays nearly independent of illumination intensity above 0.2 sun, being higher than 1.0 V at 0.2 sun for the [Cu(tmby)$_2$]$^{2+/1+}$ and [Cu(dmp)$_2$]$^{2+/1+}$ complexes. This feature gives copper complexes an intriguing potential for use in devices for diffuse light and indoor applications.

Dye Regeneration. The regeneration kinetics of the Y123 chromophor by the three copper complexes were investigated with photoinduced absorption spectroscopy (PIA). The PIA spectra for the inert electrolyte solution together with the [Cu(dmp)$_2$]$^{2+/1+}$, [Cu(dmby)$_2$]$^{2+/1+}$, and [Cu(tmby)$_2$]$^{2+/1+}$
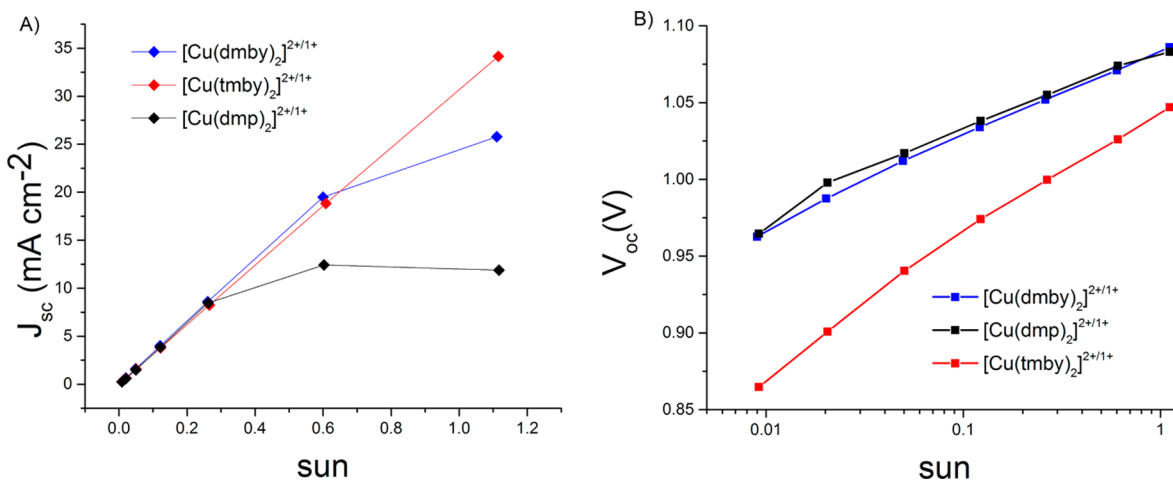
Figure 7. Light intensity dependence of (A) short-circuit current and (B) photovoltage for DSC devices based on the three different copper electrolytes.

electrolytes are given in Figure 8. Without the redox couple in the electrolyte, a bleach was observed at 540 nm due to the
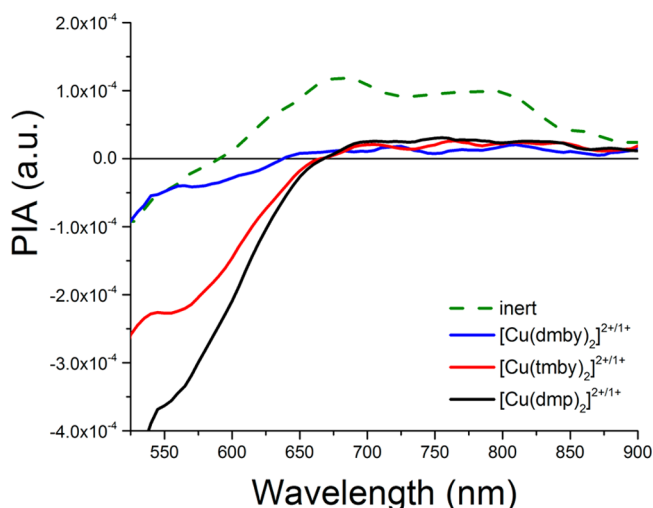

Figure 8. PIA spectra of Y123-sensitized TiO_2 with an inert electrolyte and with electrolytes prepared with the three different copper complexes.

Figure 9. Transient absorption spectroscopy measurements of Y123-sensitized TiO_2 films with inert, $[Cu(dmby)_2]^{2+/1+}$, $[Cu(tmby)_2]^{2+/1+}$, and $[Cu(dmp)_2]^{2+/1+}$ electrolytes.

ground-state bleach of the dye upon oxidation and Stark shift, i.e., absorption change of the dye as a result of changes in the electrical field across the dye molecules by the photoinjected electrons.[39,40] We also observe absorption peaks of the oxidized dye appearing at 680 and 800 nm in the absence of the copper complexes. In the spectra of copper complexes, the bleach persisted around 520 nm as a result of the Stark effect, whereas the absorption peaks of the oxidized dye disappear due to efficient regeneration of the oxidized dye molecules with the redox species. The positive signal remaining in the PIA spectra higher than 650 nm is attributed to the absorption of electrons that are accumulated in TiO_2. From the results of the PIA measurements it can be concluded that the copper complexes can effectively regenerate the oxidized dye species.

Transient Absorption Spectroscopy. Dye regeneration kinetics with the copper complexes were further investigated with nanosecond transient absorption spectroscopy (TAS) measurements, Figure 9. With an inert electrolyte (0.1 M
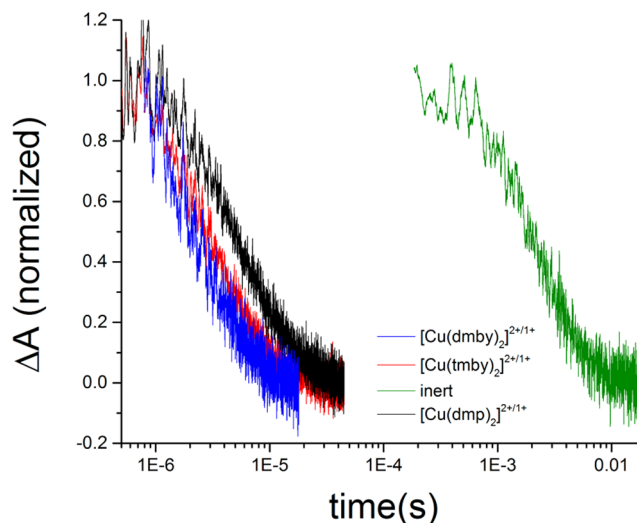
LiTFSI and 0.6 M TBP in acetonitrile), the recombination of injected electrons in the TiO_2 and oxidized dye molecules showed an absorbance decay signal with a 10 ms half-time ($\tau_{1/2}$). This is significantly slower than previously reported value for this dye which can be explained by the lower laser light intensity used in this work ($1.27\ \mu J/cm^2$) with respect to that in the reference study ($20\ \mu J/cm^2$).[10] In the presence of copper complexes, the absorbance signal shows an accelerated decay by the faster regeneration of oxidized dye molecules with Cu^{1+} species. The regeneration half-times of $[Cu(tmby)_2]^{2+/1+}$, $[Cu(dmp)_2]^{2+/1+}$, and $[Cu(dmby)_2]^{2+/1+}$ are 1.8, 2.8, and 4.8 μs, respectively, under the same conditions, showing a direct relation to the driving forces for dye regeneration. The regeneration efficiencies (Φ_{reg}) for the copper complexes are calculated using

$$\Phi_{reg} = \frac{k_{reg}}{k_{reg} + k_{rec}} \approx 1 - \frac{\tau_{1/2,redox}}{\tau_{1/2,inert}} \qquad (3)$$

For all the copper electrolytes, the Φ_{reg} values are found to be close to 100%. For the Y123 dye, the regeneration efficiencies

of cobalt ($[Co(bpy-pz)_2]^{3+/2+}$) (0.86 V vs SHE) and iodide/tri-iodide (0.37 V vs SHE) electrolytes were previously reported to be 0.93 and 0.98, respectively, based on 1.1 ms half-time for oxidized dye signal decay.[10] We can conclude that with a relatively low driving force for dye regeneration, the Cu-complexes investigated in this study provide faster kinetics compared to those of previously reported systems. The comparison of regeneration efficiencies with previously reported values for cobalt and iodide/tri-iodide indicates a better dye regeneration for copper complexes.

CONCLUSIONS

In this work, the conventional iodide/tri-iodide or cobalt based electrolytes for DSCs have very successfully been replaced with $Cu^{(II/I)}(dmby)_2TFSI_{2/1}$ (0.97 V vs SHE) and $Cu^{(II/I)}(tmby)_2TFSI_{2/1}$ (0.87 V vs SHE) complexes. These copper complexes were compared to the previously reported $[Cu(dmp)_2]^{2+/1+}$ complex by using the Y123 dye. Because of the high redox potentials of the copper electrolytes, the potential used for dye regeneration is minimized. With the given ligand structures providing small reorganization energies, the copper electrolytes are able to regenerate oxidized dye molecules with values close to unit yield even with relatively low driving forces. With the optimized devices, 10.2, 10.1, and 10.2% overall solar-to-electrical power efficiencies were recorded for $[Cu(tmby)_2]^{2+/1+}$, $[Cu(dmby)_2]^{2+/1+}$, and $[Cu(dmp)_2]^{2+/1+}$ based electrolytes, respectively, under 1000 W m^{-2} AM1.5G illumination. The photocurrent voltages are higher than 1000 mV, indicating reduced potential losses in the devices. The efficient regeneration at minimized driving forces open up possibilities for increasing DSC record efficiencies. Since the photovoltage remain high, above 1 V down to 0.2 sun light intensity, we anticipate these Cu-complex based DSCs to be particularly attractive for indoor applications. It is also clear that with an improved fill factor through a better counter electrode material the PCE values could be improved further.

ASSOCIATED CONTENT

Ⓢ Supporting Information

The Supporting Information is available free of charge on the ACS Publications website at DOI: 10.1021/jacs.6b10721.

> Synthetic procedures, cyclic voltammograms, UV−vis spectra, methods and computational details, HOMO/LUMO structures, TD-DFT results, current density versus applied potential curves, and minimum-energy structures of the Cu complexes in acetonitrile solution (PDF)

AUTHOR INFORMATION

Corresponding Author
*marina.freitag@epfl.ch

Notes
The authors declare no competing financial interest.

ACKNOWLEDGMENTS

REFERENCES

(1) O'Regan, B.; Grätzel, M. *Nature* **1991**, *353* (6346), 737.
(2) Hagfeldt, A.; Boschloo, G.; Sun, L.; Kloo, L.; Pettersson, H. *Chem. Rev.* **2010**, *110*, 6595.
(3) Tian, H.; Sun, L. *J. Mater. Chem.* **2011**, *21* (29), 10592.
(4) Yu, Z.; Vlachopoulos, N.; Gorlov, M.; Kloo, L. *Dalt. Trans.* **2011**, *40* (40), 10289.
(5) Feldt, S. M.; Gibson, E. A.; Gabrielsson, E.; Sun, L.; Boschloo, G.; Hagfeldt, A. *J. Am. Chem. Soc.* **2010**, *132* (46), 16714.
(6) Yella, a.; Lee, H.-W.; Tsao, H. N.; Yi, C.; Chandiran, a. K.; Nazeeruddin, M. K.; Diau, E. W.-G.; Yeh, C.-Y.; Zakeeruddin, S. M.; Grätzel, M. *Science (Washington, DC, U. S.)* **2011**, *334* (6056), 629.
(7) Mathew, S.; Yella, A.; Gao, P.; Humphry-baker, R.; Curchod, B. F. E.; Ashari-astani, N.; Tavernelli, I.; Rothlisberger, U.; Nazeeruddin, K.; Grätzel, M. *Nat. Chem.* **2014**, *6*, 242.
(8) Kakiage, K.; Aoyama, Y.; Yano, T.; Oya, K.; Fujisawa, J.; Hanaya, M. *Chem. Commun.* **2015**, *51* (88), 15894.
(9) Mosconi, E.; Yum, J. H.; Kessler, F.; Gómez García, C. J. G.; Zuccaccia, C.; Cinti, A.; Nazeeruddin, M. K.; Grätzel, M.; De Angelis, F. *J. Am. Chem. Soc.* **2012**, *134* (47), 19438.
(10) Yum, J.-H.; Baranoff, E.; Kessler, F.; Moehl, T.; Ahmad, S.; Bessho, T.; Marchioro, A.; Ghadiri, E.; Moser, J.-E.; Yi, C.; Nazeeruddin, M. K.; Grätzel, M. *Nat. Commun.* **2012**, *3*, 631.
(11) Feldt, S. M.; Wang, G.; Boschloo, G.; Hagfeldt, A. *J. Phys. Chem. C* **2011**, *115* (43), 21500.
(12) Feldt, S. M.; Lohse, P. W.; Kessler, F.; Nazeeruddin, M. K.; Grätzel, M.; Boschloo, G.; Hagfeldt, A. *Phys. Chem. Chem. Phys.* **2013**, *15* (19), 7087.
(13) Nelson, J. J.; Amick, T. J.; Elliott, C. M. *J. Phys. Chem. C* **2008**, *112*, 18255.
(14) Klahr, B. M.; Hamann, T. W. *J. Phys. Chem. C* **2009**, *113* (31), 14040.
(15) Sapp, S. A.; Elliott, C. M.; Contado, C.; Caramori, S.; Bignozzi, C. A. *J. Am. Chem. Soc.* **2002**, *124* (37), 11215.
(16) Gao, J.; Bhagavathi Achari, M.; Kloo, L. *Chem. Commun. (Cambridge, U. K.)* **2014**, *50* (47), 6249.
(17) Kashif, M. K.; Nippe, M.; Duffy, N. W.; Forsyth, C. M.; Chang, C. J.; Long, J. R.; Spiccia, L.; Bach, U. *Angew. Chem., Int. Ed.* **2013**, *52* (21), 5527.
(18) Bai, Y.; Yu, Q.; Cai, N.; Wang, Y.; Zhang, M.; Wang, P. *Chem. Commun.* **2011**, *47* (15), 4376.
(19) Hattori, S.; Wada, Y.; Yanagida, S.; Fukuzumi, S. *J. Am. Chem. Soc.* **2005**, *127* (26), 9648.
(20) Brugnati, M.; Caramori, S.; Cazzanti, S.; Marchini, L.; Argazzi, R.; Bignozzi, C. A. *Int. J. Photoenergy* **2007**, 1.
(21) Cong, J.; Kinschel, D.; Daniel, Q.; Safdari, M.; Gabrielsson, E.; Chen, H.; Svensson, P. H.; Sun, L.; Kloo, L. *J. Mater. Chem. A* **2016**, *4* (38), 14550.
(22) Constable, E. C.; Redondo, A. H.; Housecroft, C. E.; Neuburger, M.; Schaffner, S. *Dalt. Trans.* **2009**, No. 33, 6634.
(23) Freitag, M.; Giordano, F.; Yang, W.; Pazoki, M.; Hao, Y.; Zietz, B.; Grätzel, M.; Hagfeldt, A.; Boschloo, G. *J. Phys. Chem. C* **2016**, *120*, 9595.
(24) Tsao, H. N.; Yi, C.; Moehl, T.; Yum, J.; Zakeeruddin, S. M.; Nazeeruddin, M. K.; Grätzel, M. *ChemSusChem* **2011**, *4*, 591.
(25) McCusker, C. E.; Castellano, F. N. *Inorg. Chem.* **2013**, *52* (14), 8114.
(26) Gothard, N. A.; Mara, M. W.; Huang, J.; Szarko, J. M.; Rolczynski, B.; Lockard, J. V.; Chen, L. X. *J. Phys. Chem. A* **2012**, *116* (9), 1984.
(27) Buckner, M. T.; McMillin, D. R. *J. Chem. Soc., Chem. Commun.* **1978**, No. 17, 759.
(28) Freitag, M.; Daniel, Q.; Pazoki, M.; Sveinbjörnsson, K.; Zhang, J.; Sun, L.; Hagfeldt, A.; Boschloo, G. *Energy Environ. Sci.* **2015**, *8* (9), 2634.
(29) Ellis, H.; Vlachopoulos, N.; Häggman, L.; Perruchot, C.; Jouini, M.; Boschloo, G.; Hagfeldt, A. *Electrochim. Acta* **2013**, *107*, 45.
(30) Hoffeditz, W. L.; Katz, M. J.; Deria, P.; Cutsail, G. E.; Pellin, M. J.; Farha, O. K.; Hupp, J. T. *J. Phys. Chem. C* **2016**, *120*, 3731.

(31) Frisch, M. J.; Trucks, G. W.; Schlegel, H. B.; Scuseria, G. E.; Robb, M. A.; Cheeseman, J. R.; Scalmani, G.; Barone, V.; Mennucci, B.; Petersson, G. A.; Nakatsuji, H.; Caricato, M.; Li, X.; Hratchian, H. P.; Izmaylov, A. F.; Bloino, J.; Zheng, G.; Sonnenberg, J. L.; Hada, M.; Ehara, M.; Toyota, K.; Fukuda, R.; Hasegawa, J.; Ishida, M.; Nakajima, T.; Honda, Y.; Kitao, O.; Nakai, H.; Vreven, T.; Montgomery, J. A., Jr.; Peralta, J. E.; Ogliaro, F.; Bearpark, M.; Heyd, J. J.; Brothers, E.; Kudin, K. N.; Staroverov, V. N.; Kobayashi, R.; Normand, J.; Raghavachari, K.; Rendell, A.; Burant, J. C.; Iyengar, S. S.; Tomasi, J.; Cossi, M.; Rega, N.; Millam, J. M.; Klene, M.; Knox, J. E.; Cross, J. B.; Bakken, V.; Adamo, C.; Jaramillo, J.; Gomperts, R.; Stratmann, R. E.; Yazyev, O.; Austin, A. J.; Cammi, R.; Pomelli, C.; Ochterski, J. W.; Martin, R. L.; Morokuma, K.; Zakrzewski, V. G.; Voth, G. A.; Salvador, P.; Dannenberg, J. J.; Dapprich, S.; Daniels, A. D.; Farkas, O.; Foresman, J. B.; Ortiz, J. V.; Cioslowski, J.; Fox, D. J. *Gaussian 09*, revision E.01; Gaussian, Inc.: Wallingford, CT, 2009.

(32) Adamo, C.; Barone, V. *J. Chem. Phys.* **1999**, *110* (13), 6158.

(33) Tomasi, J.; Mennucci, B.; Cammi, R. *Chem. Rev.* **2005**, *105* (8), 2999.

(34) Marenich, A. V.; Cramer, C. J.; Truhlar, D. G. *J. Phys. Chem. B* **2009**, *113* (18), 6378.

(35) Scalmani, G.; Frisch, M. J.; Mennucci, B.; Tomasi, J.; Cammi, R.; Barone, V. *J. Chem. Phys.* **2006**, *124* (9), 094107.

(36) Sun, Z.; Zheng, K.; Li, Q.; Li, Z. *RSC Adv.* **2014**, *4*, 31544.

(37) Ørnsø, K. B.; Jónsson, E. Ö.; Jacobsen, K. W.; Thygesen, K. S. *J. Phys. Chem. C* **2015**, *119* (23), 12792.

(38) Cameron, P. J.; Peter, L. M. *J. Phys. Chem. B* **2003**, *107* (51), 14394.

(39) Cappel, U. B.; Feldt, S. M.; Schöneboom, J.; Hagfeldt, A.; Boschloo, G. *J. Am. Chem. Soc.* **2010**, *132* (26), 9096.

(40) Ardo, S.; Sun, Y.; Staniszewski, A.; Castellano, F. N.; Meyer, G. J. *J. Am. Chem. Soc.* **2010**, *132* (19), 6696.